The adhesive contact of viscoelastic spheres

G. Haïat, Minh Châu Phan-Huy, Étienne Barthel

The adhesive contact of viscoelastic spheres

G. Haiat, M.C. Phan Huy, E. Barthel*

Laboratoire CNRS/Saint-Gobain, Surface du Verre et Interfaces, BP135 39 quai Lucien Lefranc, 99303 Aubervilliers, France

We have formulated the restricted self-consistent model for the adhesive contact of linear viscoelastic spheres. This model is a generalization of both the Ting (J. Appl. Mech. 33 (1966) 845) approach to the viscoelastic contact of adhesionless spheres and the restricted self-consistent model for adhesive axisymmetric bodies. We also show how the model can be used in practice by giving a few examples of numerical solutions.

Keywords: Adhesion and adhesive; Crack propagation and arrest; Contact mechanics; Viscoelastic material; Integral transforms

1. Introduction

The contact problem as we consider it nowadays seems to have first taken shape in the last quarter of the 19th century when Hertz (1882) and Boussinesq (1885) presented solutions to the *adhesionless* contact of linear *elastic* spheres.

In the 1930s, the field of surface forces was mature enough for the problem of the *adhesion* of *rigid* bodies and its relation to the surface interactions to be tackled by Bradley (1932) and Derjaguin (1934).

In the 1960s, the problem of the *adhesionless* contact of *viscoelastic* spheres arose. The additional difficulty over the elastic case is due to the dependence of the solution upon the history of the system. In particular, the outward run (decreasing contact radius) proved difficult to solve, although a number of approaches were proposed. The definitive solution was proposed by Ting (1966), and interest in the problem waned soon afterwards.

* Corresponding author. Tel.: +33-1-48-39-55-57; fax: +33-1-48-34-74-16.
E-mail addresses: etienne.barthel@saint-gobain.com (E. Barthel).

The 1970s saw a renewed interest in the *adhesive* contact of *elastic* bodies. The famous controversy between the Russian (DMT) (Derjaguin et al., 1975) and English (JKR) (Johnson et al., 1971) schools ended when it was finally recognized that both the models were indeed limiting cases within a more general model—the restricted self-consistent model, a terminology coined by Hughes (1980), to our knowledge—in which the interactions between the surfaces are explicitly accounted for in a more physical manner (Tabor, 1977). The transition between these limit cases as the range of the interactions goes from infinity to zero was well demonstrated by numerical calculations (Muller et al., 1980, 1982; Greenwood, 1997).

In the 1990s, the first analytical model of the transition was proposed by Maugis (1992), who included the interaction between surfaces through a Dugdale model; in this model, the DMT to JKR transition is spanned when the normalized interaction parameter λ goes from zero to infinity. Soon afterwards, the usefulness of the Maugis model was evidenced in a few experimental cases (Maugis and Gauthier-Manuel, 1994; Barthel et al., 1996; Lantz et al., 1997). Simultaneously, the limitations of the Maugis model were pointed out, and the model was generalized in different ways (Barthel, 1998a, 1999; Greenwood and Johnson, 1998).

In the final years of the last century, the trend for the measurement of local mechanical properties of solids triggered interest in the *adhesive* contact of *viscoelastic* solids. Indeed, by reducing the size of the indenter, one unavoidably enters a regime in which the surface forces are significant. Thus, the coupling between mechanical response and surface interactions has to be taken into account.

It is interesting to note that the limit cases of the elastic adhesive contact problem turn out to be of limited interest in the case where the bulk response is viscoelastic. In the DMT limit (for small λ), indeed, the adhesive interaction stress is negligible compared to the mechanical compliance of the solid. As a result, in this model, the coupling between mechanical compliance and surface interactions is limited to the addition of a global adhesive force, so that the richness of the basic phenomenon cannot be accounted for. In contrast, in the JKR limit (for large λ), the gradient of the surface displacement is singular at the periphery of the contact zone, so that the strain rate is locally infinite, a shortcoming which deprives this limit of usefulness in the viscoelastic case.

Indeed, it is actually required that the viscoelastic response be taken into account to model the process zone. This was treated in depth by Schapery (1975a–c), with a view to dealing with crack extension in viscoelastic solids, and subsequently for crack healing (Schapery, 1989). His results lie at the root of further work on viscoelastic cracks by Greenwood and Johnson (1981), Johnson (1999) and Lin et al. (1999).

For the adhesive viscoelastic contact, however, the crux of the problem is to treat both the crack zone and the contact zone within a viscoelastic model. As in the adhesionless case, the formulation of the inward run (increasing contact radius) is reasonably straightforward. Hui et al. (1998) have given explicit results for the growing contact area case. In contrast, the decreasing contact radius (outward run), although of great significance, because it controls the contact rupture and thus the adherence, is still unsolved. Attard (2001a, b) has recently implemented a completely numerical model, a viscoelastic version of the full self-consistent model in the special case of an

exponential relaxation function, based on the canonical relation between the exponential function and its derivative. Lin et al. (2001) have proposed an analytical formulation, but this has up to now turned out to be of limited applicability.

In this paper, we show that the formulation of the adhesive contact of elastic bodies we proposed earlier lends itself to the description of the linear viscoelastic case as well. In addition to forming an extension of the restricted self-consistent model for the adhesion of elastic bodies, the formulas we thus obtain reduce to the results of Ting (1966) when the adhesive interaction is suppressed, thus providing a consistent description of adhesive contact problems. In particular, the decreasing contact radius case is treated on the same footing as the simpler increasing case.

We will first recall the basic equations for the restricted self-consistent model, in the linear elastic case. We then extend this approach to the linear viscoelastic case. Finally, we give an example of numerical solutions, for a strongly viscoelastic contact.

2. The restricted self-consistent model for the adhesion of elastic bodies

The self-consistent formulation of the adhesive contact problem has been reviewed recently (Huguet and Barthel, 2000). Here, we will only recall the main points:

- the gap between the surfaces geometrically depends upon the surface displacement;
- the surface displacement depends upon the surface stress through the mechanical behaviour of the solid;
- the surface stress depends, among other parameters, upon the gap through the nature of the physical interaction between the surfaces.

These three interdependent relations must be satisfied simultaneously, which results in a self-consistent solution.

2.1. The restricted self-consistent model

We now further assume that the range of the repulsive part of the interaction is much shorter than the range of the attractive part, as usually observed. This assumption leads to the *restricted* self-consistent adhesive contact problem. The boundary conditions are:

$$u(r) = \delta - f(r) \quad \text{for } r < a, \tag{1}$$

$$\sigma(r) \quad \text{known for } r > a, \tag{2}$$

where $u(r)$ is the normal surface displacement, δ is the penetration, a the radius of the contact zone and $\sigma(r)$ the surface normal stress distribution. The shape of the indenter $f(r)$ is convex and smooth but otherwise not specified.

The details of the physics of the adhesive process dictate the self-consistency equation. The diversity of the adhesive phenomena leads to different possible self-consistency equations. We here use a simple but approximate one, which is easily introduced if

the adhesive process derives from an interaction potential V between the two surfaces, though it is more general. Then, the adhesion energy is

$$w \equiv V(+\infty) - V(0) = \int_0^{+\infty} \mathrm{d}z \, \frac{\mathrm{d}V}{\mathrm{d}z} = -\int_0^{+\infty} \mathrm{d}z \, \sigma(z). \tag{3}$$

Introducing the gap

$$h(r) = u(r) - \delta + f(r) \tag{4}$$

and applying the change of variable $z = h(r)$, the self-consistency equation (Eq. (3)) is

$$w = -\int_a^{+\infty} \sigma(r) \, \frac{\mathrm{d}h(r)}{\mathrm{d}r} \, \mathrm{d}r. \tag{5}$$

The strategy for finding the solution to the self-consistent adhesive problem is to converge to a stress distribution outside the contact zone (Eq. (2)), which verifies both the boundary conditions inside the contact zone (Eq. (1)) and the self-consistency equation (Eq. (5)).

For a more detailed discussion of self-consistency equations, refer to Barthel (1998b, 1999).

Clearly, the calculation of the gap $h(r)$ from the boundary conditions (Eqs. (1) and (2)) is central to this self-consistent approach. We will now recall the main results relevant to this point.

2.2. Surface elasticity

The necessary relations for the elastic case are essentially derived from the work of Sneddon (1951, 1965) and Lowengrub and Sneddon (1965). In contrast to our recent papers, we here introduce a new function, θ, which is necessary in the viscoelastic case, but redundant with the more usual g function in the elastic case. For axisymmetric bodies, the auxiliary function g [resp. θ] is a suitable transform (of the Abel type) of the normal surface stress distribution σ [resp. the normal surface displacement u]:

$$g(s) \equiv -\int_s^{+\infty} \frac{r\sigma(r)}{\sqrt{(r^2 - s^2)}} \, \mathrm{d}r, \tag{6}$$

$$\theta(s) \equiv \frac{\mathrm{d}}{\mathrm{d}s} \int_0^s \frac{ru(r)}{\sqrt{s^2 - r^2}} \, \mathrm{d}r \tag{7}$$

$$= \left[u(s=0) + s \int_0^s \mathrm{d}r \, \frac{u'(r)}{\sqrt{(s^2 - r^2)}} \right]. \tag{8}$$

These transforms are characterized by several properties:

Prop I: they can be analytically inverted (Appendix A.1);
Prop II: $g(s)$ depends on $\sigma(r)$ for $r > s$ only, and $\theta(s)$ depends on $u(r)$ for $r < s$ only;

Prop III: under the conditions of linear elastic behaviour and the absence of shear stresses at the interface, mechanical equilibrium leads to

$$g(s) = \mathscr{K}\,\theta(s) \quad \text{for all } s, \tag{9}$$

where $\mathscr{K}$ depends upon the Young modulus E and the Poisson ratio ν as

$$\mathscr{K} = \frac{E}{2(1-\nu^2)}. \tag{10}$$

Thus, from the boundary condition Eq. (1) and Prop. II (Eq. (8)), one obtains $\theta(r)$ inside the contact zone ($r < a$):

$$\theta(r) = \delta - \delta_0(r), \tag{11}$$

where

$$\delta_0(r) = \frac{\mathrm{d}}{\mathrm{d}r}\int_0^r \frac{s f(s)}{\sqrt{(r^2-s^2)}}\,\mathrm{d}s = r\int_0^r \mathrm{d}s\,\frac{f'(s)}{\sqrt{(r^2-s^2)}} \tag{12}$$

is a signature of the shape of the indenting bodies only. Similarly, we obtain $g(r)$ outside the contact zone ($r > a$) from the boundary condition Eqs. (2) and Prop. II (Eq. (6)).

The main step in the calculation of the solution to the elastic problem is to obtain the extensions of θ and g to, respectively, outside and inside the contact zone. This step is straightforward in the elastic case because of the simplicity of the equilibrium relation Eq. (9) (Prop. III), except for the behaviour of g and θ *at* the contact zone boundary a. We will here require continuity of the $g(r)$ function (and thus of the $\theta(r)$ function), which implies continuity of the stress distribution $\sigma(r)$ (and therefore of the derivative of the displacement field $u(r)$) at $r = a$. This condition actually provides an additional equation, which we now discuss.

2.2.1. Penetration

From the specific form of θ given by Eq. (11), and the equilibrium relation Eq. (9), there results that the assumption of continuity of the stress distribution σ at the border of the contact zone a determines the penetration δ as a function of the shape of the bodies $f(r)$, the contact radius a and the attractive stress distribution outside the contact zone by

$$\delta = \delta_0(a) + \frac{1}{\mathscr{K}}\,g(a). \tag{13}$$

A problem seems to arise in the JKR case, where it is well known that the stress is discontinuous at $r = a$. However, it only appears as a limit case of models in which the continuity is obeyed (Maugis, 1992; Barthel, 1998a).

Now that θ is completely determined outside the contact zone, we can tackle the calculation of the gap.

2.2.2. The gap and the self-consistency equation

From the inverse of Eq. (7), Eq. (A.3), in Appendix A, the surface displacement can be split into

$$u(r) = \frac{2}{\pi}\int_0^a \mathrm{d}s\,\frac{\theta(s)}{\sqrt{r^2-s^2}} + \frac{2}{\pi}\int_a^r \mathrm{d}s\,\frac{\theta(s)}{\sqrt{r^2-s^2}}. \tag{14}$$

It can be shown that a convenient form for the gap (see Appendix A.2) is

$$h(r) = h_{\mathrm{Hertz}}(r,a) + \frac{2}{\pi}\int_a^r \frac{\theta(s)-\theta(a)}{\sqrt{r^2-s^2}}\,\mathrm{d}s \tag{15}$$

with

$$h_{\mathrm{Hertz}}(r,a) = \frac{2}{\pi}\frac{1}{R}\,f_{\mathrm{H}}(r,a), \tag{16}$$

where

$$f_{\mathrm{H}}(r,a) \equiv \int_a^r \mathrm{d}s\,\frac{(s^2-a^2)}{\sqrt{r^2-s^2}} = \left\{\frac{a}{2}\sqrt{r^2-a^2} + \left(\frac{r^2}{2}-a^2\right)\arccos\left(\frac{a}{r}\right)\right\}. \tag{17}$$

This form of the gap will be used below to compute the self-consistency equation in a special case, the general expression being too complex to be of real use.

In addition, from this formulation (Eq. (15)), it becomes apparent that, as noted above, the continuity of θ entails the suppression of the square root singularity of the gap h at a (cf. Appendix A.2).

2.2.3. Force

Similarly, the total force,

$$F = 4\int_0^{+\infty} \mathrm{d}r\,g(r) \tag{18}$$

can be split into two terms. The outer term is

$$F_{\mathrm{ext}} = 4\int_a^{+\infty} \mathrm{d}r\,g(r). \tag{19}$$

The inner term is

$$F_{\mathrm{int}} = 4\int_0^a \mathrm{d}r\,g(r) = 4\mathscr{K}(a\delta - \phi_0(a)) \tag{20}$$

$$= F_{\mathrm{H}}(a) + F_{\mathrm{JKR}}(a) \tag{21}$$

with

$$F_{\mathrm{H}}(a) = 4\mathscr{K}(a\delta_0(a) - \phi_0(a)), \tag{22}$$

$$F_{\mathrm{JKR}}(a) = 4ag(a), \tag{23}$$

where F_{H} is the non-adhesive Hertz force which, like the function

$$\phi_0(r) \equiv \int_0^r \mathrm{d}s\,\delta_0(s) \tag{24}$$

depends only upon the shape of the indenter, and F_{JKR} is the corrective JKR-like flat punch term.

2.2.4. Resolution of the adhesive contact problem

In the experiments, two main possibilities are met, where the displacement (fixed grip) or the force (fixed load) are prescribed. Assuming a self-consistent model as in Eq. (5), the problem is thus to determine the contact radius a and the attractive stress distribution by

(a) in a fixed grip experiment, solving the displacement (Eq. (13)) and self-consistency (Eq. (5)) equations simultaneously, and then calculating the force;
(b) in a fixed load experiment, solving the force (Eq. (18)) and self-consistency (Eq. (5)) equations simultaneously and then calculating the displacement.

Examples of such procedures can be found in Barthel (1998b, 1999) and Greenwood and Johnson (1998).

3. Adhesion of viscoelastic bodies

3.1. Linear viscoelastic behaviour

Assuming the simplest viscoelastic behaviour—a constant Poisson ratio—the stress σ and deformation ε now obey

$$\sigma(t) = \int_0^t \mathrm{d}\tau\, \psi(t-\tau) \frac{\mathrm{d}}{\mathrm{d}\tau}\, \varepsilon(\tau), \tag{25}$$

$$\varepsilon(t) = \int_0^t \mathrm{d}\tau\, \phi(t-\tau) \frac{\mathrm{d}}{\mathrm{d}\tau}\, \sigma(\tau), \tag{26}$$

where the relaxation function $\psi(t)$ and the creep function $\phi(t)$ are inverse for this product of convolution. Therefore we have

$$\sigma(t) = \sigma(t_0) + \int_{t_0}^t \mathrm{d}\tau\, \psi(t-\tau) \frac{\partial}{\partial\tau} \int_{t_0}^\tau \mathrm{d}\tau' \phi(\tau-\tau') \frac{\partial}{\partial\tau'}\, \sigma(\tau') \tag{27}$$

provided $\sigma(t)$ is independent of time for $t < t_0$.

Since there is no coupling through the response functions ψ and ϕ between the temporal and spatial variations of the physical quantities, the equilibrium equation (Eq. (9)) for the adhesive contact between a rigid indenter and a viscoelastic solid reads

$$g(t) = \int_0^t \mathrm{d}\tau\, \psi(t-\tau) \frac{\mathrm{d}}{\mathrm{d}\tau}\, \theta(\tau) \tag{28}$$

or its inverse

$$\theta(t) = \int_0^t \mathrm{d}\tau\, \phi(t-\tau) \frac{\mathrm{d}}{\mathrm{d}\tau}\, g(\tau). \tag{29}$$

The essential Eqs. (5), (13), (15), and (18) remain unaltered, except for the introduction of the time dependence. For instance, the self-consistency equation Eq. (5) now reads

$$w = \int_{a(t)}^{+\infty} \sigma(r,t) \frac{\mathrm{d}}{\mathrm{d}r}\, h(r,t)\, \mathrm{d}r. \tag{30}$$

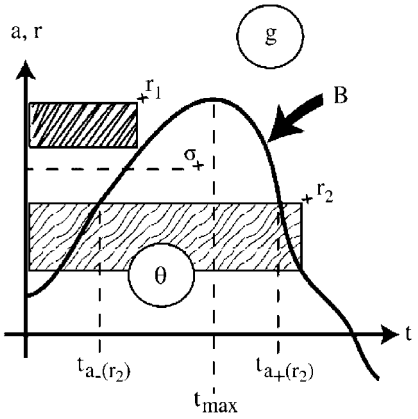

Fig. 1. Schematic plot of contact radius vs. time (line B). The r–t plane is divided into two parts: the g-domain ($a(t) < r$), in which the (attractive) surface stress distribution is known, and the θ-domain ($r < a(t)$), where the surface displacement is known. A solution is a time dependent-stress distribution which verifies the penetration equation (Eq. (31)) [resp. Eq. (4)] for $t < t_{\max}$ [resp. $t_{\max} < t$]) and the self-consistency equation (Eq. (30)). The shaded rectangles exemplify the r–t zones relevant for the calculation of the gap at r_1 (inward) and r_2 (outward). Like the penetration, calculation of the stress inside the contact zone (σ point) is done along a horizontal line. The functions $t_{a\_}(r)$ and $t_{a+}(r)$ are defined in the text (Eqs. (34) and (43)).

The guideline to establishing the adhesive viscoelastic contact equations is thus to express these equations at time t as a function of known quantities at time $\tau < t$. However, for a given $\tau < t$, we directly know $\theta(r, \tau)$ for $r < a(\tau)$ only (from the datum of $\delta(\tau)$ and $\delta_0(r)$) and $g(r, \tau)$ for $a(\tau) < r$ only. This defines two time–space domains, the g- [resp. θ-] domain where g [resp. θ] is known (Fig. 1). The calculation of the extensions of each function (g in the θ-domain and conversely) is now more complex, because the simple proportionality relation Eq. (9) is replaced by Eq. (28) or its inverse Eq. (29), which sometimes must be used recursively, leading to cumbersome nested temporal integrals.

We will therefore restrict ourselves to the two cases which are most significant: for (a) increasing and (b) subsequently decreasing contact radius. Indeed, as in the adhesionless case, for more complex loading histories, the equations which describe the response of the system become increasingly unwieldy, although they can still be derived with the methods developed in the present paper.

The next two sections will briefly present the general results for the viscoelastic adhesive contact, while the rest of the paper is devoted to the explicit development of a special case as an example.

3.2. Increasing contact radius

This is the most straightforward case, since the history of the system is simple enough to easily be taken into account: for a given radius r, we meet at most once with the

boundary B between the two domains (Fig. 1). Except for the stress distribution inside the contact zone, and thus the force (Section 3.2.4), all relevant quantities can be expressed with one single temporal integral.

3.2.1. Displacement

From Eq. (29), the continuity of θ at the edge of the contact zone, which determines δ, now yields

$$\delta(t) = \delta_0(a(t)) + \int_0^t \mathrm{d}\tau\, \phi(t-\tau)\, \frac{\partial}{\partial \tau}\, g(a(t),\tau), \tag{31}$$

which is the form of Eq. (13) valid for the viscoelastic case in the increasing contact radius regime.

3.2.2. The gap

Now in the gap equation Eq. (15), we have

$$\theta(r,t) = \int_0^t \mathrm{d}\tau\, \phi(t-\tau)\, \frac{\partial}{\partial \tau}\, g(r,\tau) \tag{32}$$

and thus

$$h(r,t) = h_{\mathrm{Hertz}}(r,t) + \frac{2}{\pi} \int_0^t \mathrm{d}\tau\, \phi(t-\tau)\, \frac{\partial}{\partial \tau} \int_{a(t)}^r \mathrm{d}s\, \frac{g(s,\tau) - g(a(t),\tau)}{\sqrt{r^2 - s^2}} \tag{33}$$

from which the self-consistency equation is derived through Eq. (30).

3.2.3. The stress distribution inside the contact zone

Inside the contact zone ($r < a(t)$), the stress distribution can be calculated from the successive use of Eqs. (28) and (11). However, in Eq. (28), the time domain extends from 0 to t, while $\theta(r,t)$ is known only inside the θ-domain, that is between $t_{a\_}(r)$ and t, where $t_{a\_}(r)$ is defined in the increasing contact radius zone (Fig. 1) by

$$a(t_{a\_}(r)) = r. \tag{34}$$

Therefore, outside the θ-domain, we have to express $\theta(r,\tau)$ as a function of $g(r,\tau')$ through Eq. (29), from which the following nested integral expression results:

$$\begin{aligned} g(r,t) = &\int_{t_{a\_}(r)}^t \mathrm{d}\tau\, \psi(t-\tau)\, \frac{\partial}{\partial \tau} \{\delta(\tau) - \delta_0(r)\} \\ &+ \int_0^{t_{a\_}(r)} \mathrm{d}\tau\, \psi(t-\tau)\, \frac{\partial}{\partial \tau} \int_0^\tau \mathrm{d}\tau'\, \phi(\tau-\tau')\, \frac{\partial}{\partial \tau'}\, g(r,\tau'). \end{aligned} \tag{35}$$

Note that this expression is actually also valid in the decreasing contact radius regime, where it lies at the root of the equation giving the penetration.

3.2.4. The force

The total force

$$F(t) = F_{\mathrm{ext}}(t) + F_{\mathrm{int}}(t) \tag{36}$$

is the sum of the outer term

$$F_{\text{ext}}(t) = 4 \int_{a(t)}^{\infty} \mathrm{d}r\, g(r) \tag{37}$$

and the inner terms

$$F_{\text{int}}(t) = F_{\text{int},a}(t) + F_{\text{int},b}(t) \tag{38}$$

with

$$F_{\text{int},a}(t) = 4 \int_0^t \mathrm{d}\tau\, \psi(t-\tau) \frac{\mathrm{d}}{\mathrm{d}\tau} \int_0^{\min(a(t),a(\tau))} \mathrm{d}r\, (\delta(\tau) - \delta_0(r)) \tag{39}$$

and, in a manner similar to the previous paragraph,

$$F_{\text{int},b}(t) = 4 \int_0^{t_{a\_}(a(t))} \mathrm{d}\tau\, \psi(t-\tau) \frac{\mathrm{d}}{\mathrm{d}\tau} \int_0^{\tau} \mathrm{d}\tau'\, \phi(\tau-\tau') \frac{\mathrm{d}}{\mathrm{d}\tau'} \int_{a(\tau)}^{a(t)} \mathrm{d}r\, g(r,\tau'). \tag{40}$$

Here again, the expression for the force is valid for both in- and outward runs.

3.3. Decreasing contact radius

In the decreasing contact radius regime, we may meet up to twice with the boundary B (Fig. 1), from which increasingly complex expressions result.

3.3.1. Displacement

Using Eq. (35), continuity of g at the periphery of the contact now gives

$$\begin{aligned} g(a(t),t) = &\int_{t_{a\_}(a(t))}^{t} \mathrm{d}\tau\, \psi(t-\tau) \frac{\partial}{\partial\tau} \{\delta(\tau) - \delta_0(a(t))\} \\ &+ \int_0^{t_{a\_}(a(t))} \mathrm{d}\tau\, \psi(t-\tau) \frac{\partial}{\partial\tau} \left(\int_0^{\tau} \mathrm{d}\tau'\, \phi(\tau-\tau') \frac{\partial}{\partial\tau'} g(a(t),\tau') \right), \end{aligned} \tag{41}$$

which is the form of Eq. (13) valid in the decreasing contact radius regime. We note that this equation is simply an extension of the integral equation characteristic of the decreasing contact radius case in the adhesionless contact (Ting, 1966), which is recovered here for $g = 0$. Thus, as in the non-adhesive case, the penetration δ is to be calculated from this integral equation.

In addition, we note that at $t = t_{a\_}(a(t))$, that is to say when the contact radius reaches its maximum $a_{\max} = a(t_{\max})$, the second term on the right-hand side of Eq. (41) is shown through Eq. (27) to equal $g(a(t),t)$. Thus the convolution integral of $\delta(\tau)$ is zero, with the simple but prominent implication that $\delta(t)$ is continuous at $t_{\max}$.

3.3.2. The gap and the self-consistency relation

In the calculation of the gap, for a given radius we meet twice with the boundary B between domains, leading to an increasing number of nested temporal integrals. As an example of the recursive use of Eqs. (28) and (29) already applied in Section 3.2.3, we here explicitly give the suitable expression for θ to calculate the gap, in which each

term is expressed as a function of known quantities (the displacement in the θ-domain, the stress distribution in the g-domain):

$$\theta(s,t) = \int_0^{t_{a_-}(s)} \mathrm{d}\tau\, \phi(t-\tau)\, \frac{\partial}{\partial \tau}\, g(s,\tau) + \int_{t_{a_+}(s)}^{t} \mathrm{d}\tau\, \phi(t-\tau)\, \frac{\partial}{\partial \tau}\, g(s,\tau)$$
$$+ \int_{t_{a_-}(s)}^{t_{a_+}(s)} \mathrm{d}\tau\, \phi(t-\tau)\, \frac{\partial}{\partial \tau} \left\{ \int_{t_{a_-}(s)}^{\tau} \mathrm{d}\tau'\, \psi(\tau-\tau')\, \frac{\partial}{\partial \tau'}\, \theta(s,\tau') \right.$$
$$\left. + \int_0^{t_{a_-}(s)} \mathrm{d}\tau'\, \psi(\tau-\tau')\, \frac{\partial}{\partial \tau'} \int_0^{\tau'} \mathrm{d}\tau''\, \phi(\tau'-\tau'')\, \frac{\partial}{\partial \tau''}\, g(s,\tau'') \right\}, \tag{42}$$

where $t_{a_+}(r)$ is defined in the decreasing contact radius zone (Fig. 1) by

$$a(t_{a_+}(r)) = r. \tag{43}$$

Inverting the order of the temporal and the spatial integrals, we obtain an expression for u where all terms can be calculated as a function of the history of the system. Here again, from the gap expression, the self-consistency equation is derived through Eq. (30). These expressions are given explicitly in Appendix B (Eq. (B.42)).

3.4. The resolution of the adhesive viscoelastic contact problem

In this case, the solution proceeds as follows: one has to simultaneously solve the penetration equation (Eqs. (31) or (41) —the latter one being an integral equation) [resp. the force equation (Eq. (36))] and the self-consistency equation Eq. (30) for a fixed grip [resp. fixed load] experiment. We now show that this approach is feasible in practice with the following examples.

4. Double–Hertz model

To model experiments with a sphere, we assumed a paraboloidal shape of the indenter. Other shapes can naturally be dealt with, and nano-indentation addicts may here assume a sphere-terminated cone, and modify δ_0 and ϕ_0 accordingly. As for the interaction zone, we at first implemented a Dugdale model. The resulting model was thus the viscoelastic Dugdale–Maugis model. In practice however, we found it much more advantageous to avail ourselves of the so called 'double-Hertz' model, put forward by Greenwood and Johnson (1998), where the attractive stress distribution inside the *interaction* zone, bounded by the contact radius a and the interaction radius c, is assumed to be ellipsoidal. Indeed, in this model, we benefit both from the absence of stress discontinuity at the periphery of the *interaction* zone and from the analyticity of all the spatial integrals. As a result, the numerical calculations are significantly easier. All the equations used are given explicitly in Appendix B.

A program has been implemented to work with any pair of viscoelastic functions, provided they are inverse for the convolution integrals Eqs. (28) and (29). In the

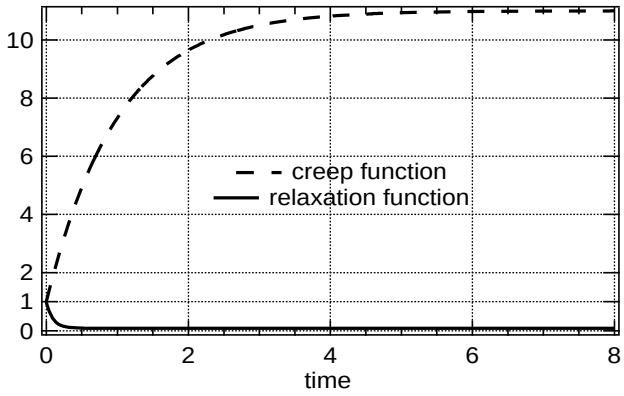

Fig. 2. Exponential creep (Eq. (44)) and relaxation (Eq. (45)) functions used for the results shown below. The characteristic creep time is the time unit, and the characteristic creep parameter is $k = 0.09$.

following, we assume a normalized standard viscoelastic solid model with creep and relaxation functions given by

$$\phi(t) = 1 + \frac{k}{1-k}\,(1 - \exp(-t)), \tag{44}$$

$$(t) = k + (1-k)\exp(-t/k), \tag{45}$$

where k is the characteristic parameter of the normalized creep process. The relaxation and creep functions for $k = 0.09$, as assumed below, are illustrated in Fig. 2. Note that for this value of k, the relaxed modulus is about ten times smaller than the instantaneous modulus.

As mentioned in the Introduction, in normalized form, in the elastic case (paraboloidal indenter with radius R, adhesion energy w: see Eqs. (B.19)–(B.22) for the details of the normalization), the adhesive interaction is characterized by a single parameter λ. We here use the same normalization, where the instantaneous modulus $\psi(0)$ is now substituted for the elastic modulus.

As an example, let us assume $\psi(0)=100$ MPa, $R=2$ cm and $w=50$ mJ m^{-2}; we then have the following normalizing factors: force, $P_0 \simeq 3$ mN; contact radius, $A_0 \simeq 90$ μm; penetration: $\Delta_0 \simeq 0.4$ μm and stress: $\sigma_0 \simeq 0.4$ MPa.

In the following section, we discuss numerical results obtained for an adhesion parameter $\lambda = 4$. Thus, we present examples for a rather extreme (and computationally more demanding) case of notably viscous solid with sizeable adhesion.

We assume a fixed grip experiment, and simultaneously solve Eqs. (B.30) and (B.37) (inward run), or (B.38) and (B.56) (outward run), for the normalized radius of the contact zone $A(t)$ and the normalized radius of the interaction zone $C(t)$. We suppose zero penetration and an instantaneous switch-on of the interactions at $t=0$. The temporal integrals were calculated with a Simpson rule method, with a convergence criterion of 10^{-4}. The three-integrals term has been neglected throughout, due to long computation times. We checked in a few cases that inclusion of this term leads to minor changes

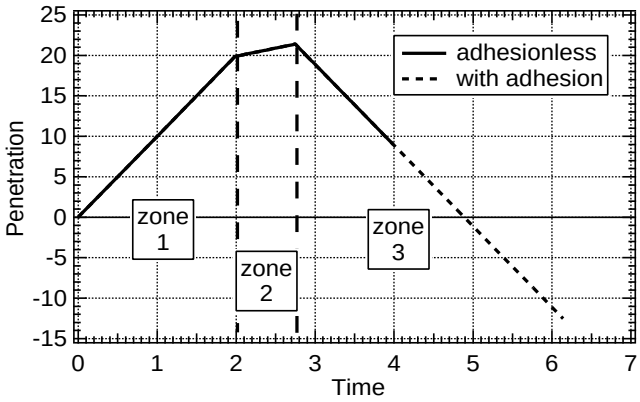

Fig. 3. Example 1—Penetration history imposed on the system. Inward (fast (+10): zone 1—slow (+2): zone 2) and outward (fast (−10): zone 3) normalized penetration velocities.

in the contact radius history at the turning point (maximum contact radius), and is not significant at later stages.

4.1. Numerical results

4.1.1. Example 1: adhesionless contact—adhesive contact

We here contrast the adhesive and adhesionless systems. The indenter is driven with a simple penetration history (Fig. 3) with a penetration velocity of +10 (inward part of the curve—zone 1) or −10 (outward—zone 3), normalized to the characteristic creep time. An intermediate period of reduced penetration velocity (+2—zone 2) is provided for, so as to better illustrate the response of the system.

Between these two cases, the main difference in the inward part of the run (zones 1 and 2) lies in the contact radius (Fig. 4), which, for an identical penetration, is increased through the interactions. However, in the inward run, the force curves for the two cases are quite similar, featuring in particular a sharp relaxation process in zone 2 (Fig. 5). The one noteworthy difference is to be found at the very beginning of the curve, where the initially adhesive (i.e. negative) total force, in the adhesive case, swiftly decays into repulsive.

In the third zone, the overall differences between the two cases are more striking. When the sphere is retracted, a sharp decrease of the contact radius (Fig. 4) to zero occurs for the adhesionless contact, while the contact radius goes on increasing and then stays roughly constant for one unit of time when adhesion is present, before it finally bends down. In the constant contact radius region, the force vs. penetration curve (Fig. 6) is found to be linear. Finally, the maximum tensile force is −13.4, considerably larger than the bare −1.5 expected in an elastic model for such a large value of λ. Thus in the viscoelastic case, the contact rupture is characterized by two parameters: the "stick time" between the inception of retraction and the decrease of the contact radius, and the (large) adhesive force.

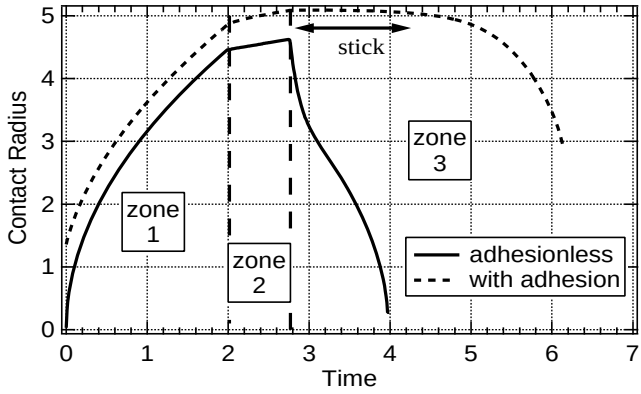

Fig. 4. Example 1—Contact radius as a function of time. In zones 1 and 2, the contact radius increases under the effect of the interactions, in a manner similar to the classical elastic contact. In zone 3 (outward), in the adhesive contact, the contact radius stays roughly constant for about one time unit before curving down, in sharp contrast to the adhesionless case. We will call this constant contact radius domain the "stick" domain.

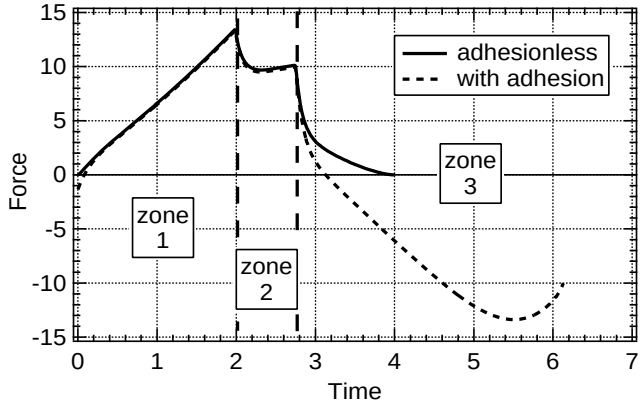

Fig. 5. Example 1—Force as a function of time. In the adhesive and adhesionless cases, the forces are similar in zones 1 and 2 (inward), due to fast stress relaxation, most evident in zone 2. In the adhesive case however, the contact zone starts receding (in zone 3) only if sufficient tensile stresses have built up in the contact zone, which results in a large adhesive force.

4.1.2. Example 2: influence of the retraction velocity

In the second series of calculations, we changed the retraction velocity, for identical inward runs (Fig. 7). The stick time increases markedly when the retraction velocity decreases (Fig. 8). The adhesive force (Fig. 9), however, is little affected (an apparent dependence as the power 0.1 of the contact radius velocity at maximum tensile force). This behaviour, which cannot be explained by crack tip effects only, will be qualitatively explained in the discussion.

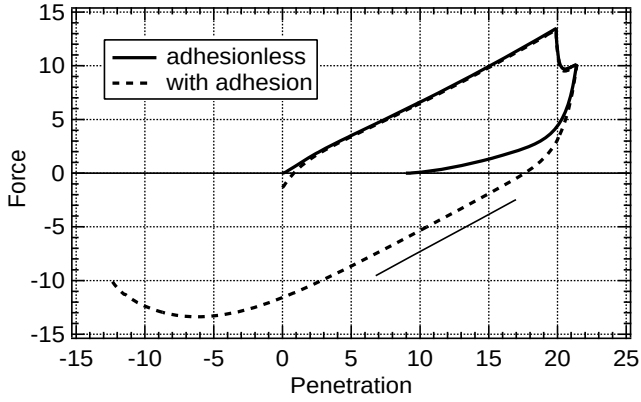

Fig. 6. Example 1—Force as a function of penetration: note the linear regime in the "stick" domain. The theoretical slope for a flat punch with the relaxed modulus (Eq. (46)) is indicated by the line segment under the curve.

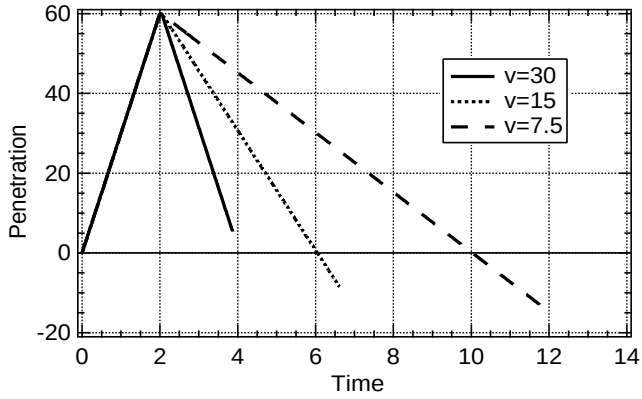

Fig. 7. Example 2—Penetration history imposed on the system. An identical fast inward run is followed by retraction at three different velocities.

4.1.3. Example 3: shallower indents

Everyday experience or laboratory experiments evidence an increase of the adhesive force with dwell time or maximum penetration depth. The present system features such a behaviour as well. Using the penetration velocities displayed in Fig. 10, decreasing the maximum penetration, which occurs at $t = 2$, from 20 to 6, the maximum contact radius (Fig. 11) drops from about 5 to about 3, and with identical retraction velocities, we calculate a decrease of the adherence force (Fig. 12) from 13.1 to 8.6.

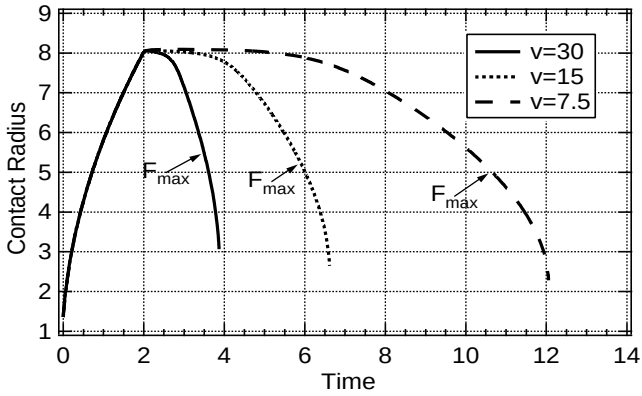

Fig. 8. Example 2—Contact radius as a function of time. The points at which the maximum tensile (i.e. adherence) force is reached are indicated. Note the variation of the "stick time" with retraction velocity (see text for a qualitative analysis).

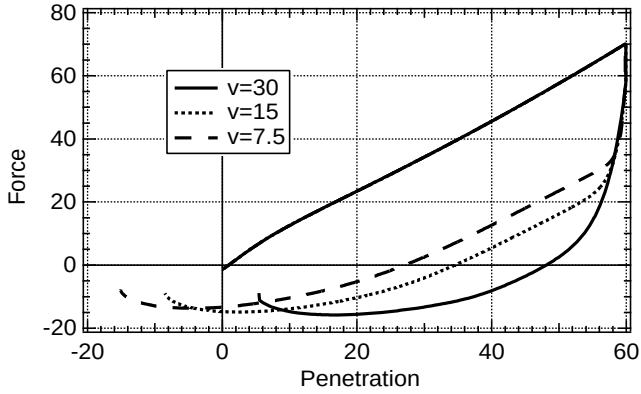

Fig. 9. Example 2—Force as a function of penetration. A weak decrease of the adherence force with decreasing retraction velocity (-15.8 for $v=30$, -14.9 for $v=15$, -13.7 for $v=7.5$) is calculated, while the penetration decreases markedly, to negative values for the two slower velocities, because of the competition between creep under mainly compressive (zones 1 and 2) or mainly tensile (zone 3) stresses.

4.2. Discussion

4.2.1. Crack tip effects—creep

The typical size of the interaction zone is of the order 5×10^{-2}, to be compared with the 8×10^{-2} expected for an elastic solid with the instantaneous modulus. Typical contact radius velocities are in the range 1–4, except in the stick zone, where it goes to zero. Thus, in the crucial zones—zone 1, which determines the maximum contact radius, and the rupture zone (later stage of zone 3)—, the characteristic time of the interaction stress is of the order of a few 10^{-2}, well below the creep time (unity). As

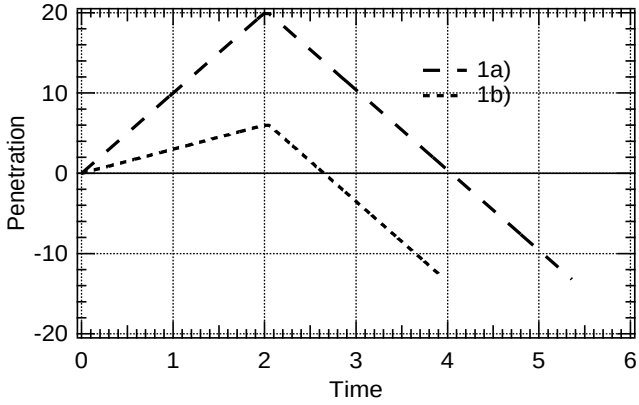

Fig. 10. Example 3—Penetration history imposed on the system: identical retraction velocity, but two different maximum penetrations.

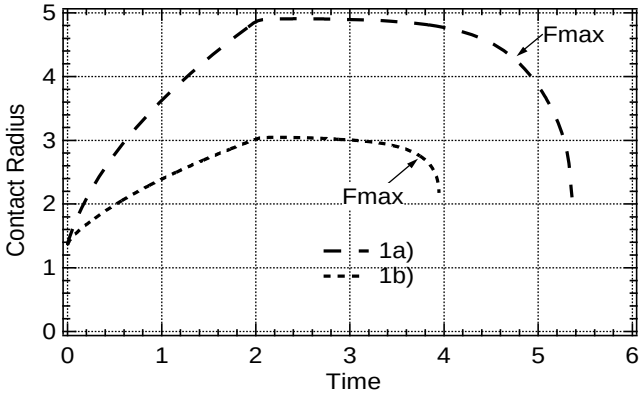

Fig. 11. Example 3—Contact radius as a function of time. The points at which the maximum tensile (i.e. adherence) force is reached are indicated.

a result, the interaction zone behaves essentially elastically, with an effective modulus close to the instantaneous value. It is only in the stick zone (constant contact radius) that, due to reduced crack tip velocities, viscoelastic crack tip effects become apparent mainly under the form of a slow increase of the contact radius, due to creep, while the interaction zone contracts by a factor of the order of unity (Fig. 13), because the solid is effectively softer at long time scales.

4.2.2. Contact zone effects—stress relaxation

On the other hand, most of the effects described above may be ascribed to stress relaxation within the contact zone. This relaxation is particularly noticeable in zone 2, where the force decay has a fitted characteristic time of 0.089 (Fig. 5), to be compared

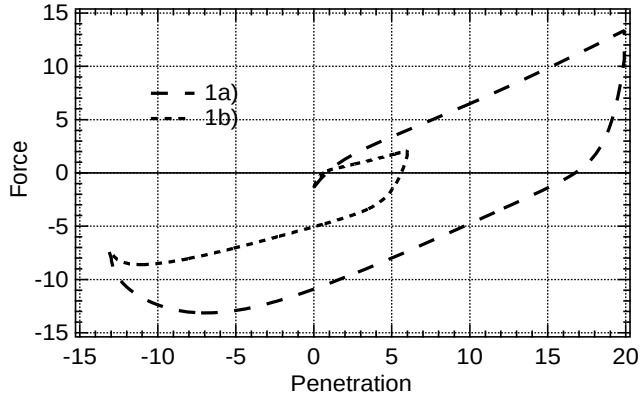

Fig. 12. Example 3—Force as a function of penetration. The weaker adherence force (-8.6 vs. -13.1) is due to the smaller maximum contact radius: for small penetrations, the contact radius relevant for the calculation of the adherence force is mainly controlled by the maximum contact radius.

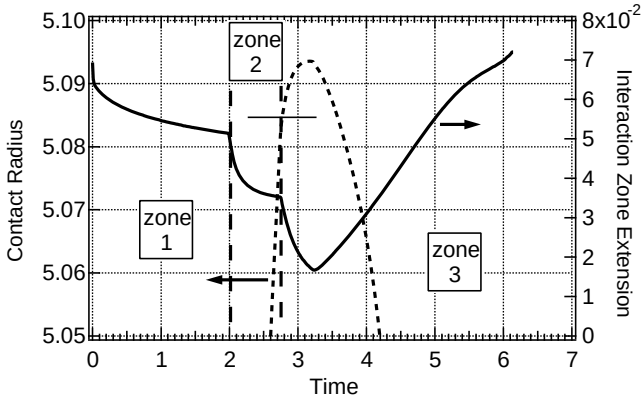

Fig. 13. Evidence for crack tip effects (taken from Example 1). The contact zone radius (dashed—left-hand scale, note the high magnification) continues increasing well into the decreasing displacement zone (zone 3) as a result of creep at the crack tip. The interaction zone extension $c - a$ (line—right-hand scale) decreases—weakly—with decreasing crack tip velocity $\mathrm{d}a/\mathrm{d}t$.

with the theoretical $k = 0.09$ (Eq. (45)). Similarly, in the region where the contact radius is about constant, the stresses relax rapidly and the system actually behaves as a flat punch of radius equal to the contact radius a with a modulus equal to the infinite-time modulus K_∞. Indeed, in this case, the predicted slope (or contact stiffness) is

$$\kappa = \tfrac{3}{2} K_\infty a, \tag{46}$$

which in the present case is equal to 0.69, identical to the slope in the calculated solution. Similarly, the stick zone, where the contact radius is constant, results from the weak elastic energy build-up in the contact zone. It is only for a sizeable backward

displacement that tensile stresses at the crack tip finally meet up with the adhesive interactions. The stick time can thus be estimated from the following argument: in Eq. (41), the integral

$$I = \int_{t_{a\_}(a(t))}^{t} \mathrm{d}\tau\, \psi(t-\tau)\, \frac{\partial}{\partial \tau}\{\delta(\tau) - \delta_0(a(t))\} \tag{47}$$

is an expression of (the Abel transform of) the stress at $a(t)$ induced by the retraction motion $\delta(\tau)$, where the last (double-integral) term has been neglected. It has to equal the (Abel transform of the) stress generated by the interactions, which is $g(a(t))$. Now, taking rather arbitrarily an interaction zone size of 4×10^{-2}—not quite the elastic limit, since we are still in a low crack velocity region (Fig. 13), a contact radius of 8, Eq. (B.23) yields a value $g(a(t)) \simeq 3$. Now, during the "stick" phase, the penetration is monotonously decreasing. Then, taking into account the present form for the relaxation function Eq. (45), for $k \ll 1$,

$$I \simeq k\, \frac{\mathrm{d}\delta}{\mathrm{d}t} \left(t - t_{\max} + 1 - \exp\left(-\frac{t - t_{\max}}{k} \right) \right). \tag{48}$$

From this equation and $g(a(t)) = 3$, we estimate that $t - t_{\max}$ is, respectively, 0.2, 1 and 3 for penetration velocities of 30, 15 and 7.5, in reasonable agreement with the stick times observed in Fig. 8.

Along the same line of thought, in the outward run, reduction of the crack size requires the build-up of sufficient tensile stresses inside the contact zone. However, in contrast to an elastic behaviour, where compressive and tensile stresses evolve simultaneously, in the viscoelastic case, the compressive contact zone stresses have relaxed and tensile stresses dominate in the outward leg. Thus, the balance between compressive and tensile stresses found in the elastic case is offset for a viscoelastic contact, which entails an adhesive force much larger than expected in a completely elastic problem, along with a reduced release of elastic energy. Thus, stress relaxation inside the contact zone is the main source of energy dissipation.

More precisely, in a JKR-like regime, where the interaction zone is small, the force is dominated by the inner term in

$$P \simeq \frac{3}{2} \int_0^t \mathrm{d}\tau\, \tilde{\psi}(t-\tau)\, \frac{\mathrm{d}}{\mathrm{d}\tau} \left(A(t) \Delta(\tau) - \frac{A(t)^3}{3} \right), \tag{49}$$

while

$$G(A) \simeq \int_0^t \mathrm{d}\tau\, \tilde{\psi}(t-\tau)\, \frac{\mathrm{d}}{\mathrm{d}\tau} (\Delta(\tau) - A(t)^2), \tag{50}$$

which combine to give an expression quite similar to the one proposed by Johnson (1999):

$$P \simeq \tilde{\psi}(t) A(t)^3 + \tfrac{3}{2} G(A(t)) A(t) \tag{51}$$

with

$$G(A) = -\frac{\pi}{3}\, \lambda \sqrt{C^2 - A^2}. \tag{52}$$

If the interaction zone may be modelled as elastic, then

$$1 \simeq \frac{\pi^2}{12}\,\lambda^2(C(t) - A(t)). \tag{53}$$

Assuming fast stress relaxation,

$$(t) \simeq \psi(+\infty) \tag{54}$$

and

$$P \simeq \psi(+\infty)A(t)^3 - \sqrt{6}A(t)^{3/2}, \tag{55}$$

which is the normalized JKR equation with relaxed Hertzian stresses. The maximum force is obtained for a radius

$$A_{Pm} = \frac{1}{(+\infty)^{2/3}}\left(\frac{3}{2}\right)^{1/3} \tag{56}$$

and is

$$P_{\max} = -\frac{1}{(+\infty)}\,\frac{3}{2}. \tag{57}$$

In our example, this approximation results in an adherence force $P_{\max}$ equal to -16.7, and a contact radius at the maximum force A_{Pm} of 5.7, consistent with the values computed for large penetrations (Example 2).

What happens, then, for penetrations smaller than A_{Pm} (Example 3)? The contact radius at maximum tensile force is of course no longer given by Eq. (56). It is not exactly given by the maximum contact radius either because the interaction zone extension, and $|g(a)|$, increase when the contact radius velocity increases. However, at the same time, the contact radius decreases. It is a balance of these two competing effects which determines the contact radius at maximum tensile force. The approximation (Eq. (55)) may still be useful, however. Indeed, substituting the calculated contact radius values in Eq. (55), we obtain approximate adherence forces of, respectively, -9.3 and -14.7 for computed values of -8.6 and -13.1.

5. Conclusion

In the first part of the paper, we have shown that the restricted self-consistent model for the adhesive contact of linear elastic bodies lends itself to generalization to linear viscoelasticity. In the relatively simple model developed in the present paper, two scalar equations (expressing the continuity of the stress distribution at the contact zone boundary and the self-consistency of the description of the adhesive stresses) have to be solved simultaneously for the contact zone radius and the interaction zone extension as a function of time. Complex histories of the contact radius lead to increasing numbers of nested time integrals in these equations, with decreasing practical utility for numerical calculations.

In the second part of the paper, a case study, we chose a highly viscoelastic response. We then evidence a “pinning” of the contact zone in the initial stages of the penetration

decrease. This "sticking" phenomenon is due to the fast relaxation of the stresses (both compressive and tensile) inside the contact zone, so that crack back-propagation requires the renewal of tensile stresses inside the contact zone, as described by Eq. (48). As a result, the adherence force is magnified because the tensile stresses needed for crack retraction are no longer balanced by equivalent compressive stresses, since the latter have already relaxed (Eq. (55)). Thus, we find that the amplification of the adherence force occurs because strain and stress inside the contact zone are out of phase, as typical of viscoelasticity. Crack tip effects play a more subdued role.

Ongoing work deals with the development of approximate models and the incorporation of roughness therein.

Appendix A. General relations

A.1. Inversion of the auxiliary functions g and θ

The inverse relations to Eqs. (6) and (7) are:

$$s\sigma(s) = -\frac{2}{\pi}\frac{\mathrm{d}}{\mathrm{d}s}\int_s^{+\infty} \mathrm{d}r\, \frac{rg(r)}{\sqrt{(r^2-s^2)}} \tag{A.1}$$

or

$$\sigma(s) = \frac{2}{\pi}\left[\int_s^{+\infty} \mathrm{d}r\, \frac{g'(r)}{\sqrt{(r^2-s^2)}}\right] \tag{A.2}$$

and

$$u(r) = \frac{2}{\pi}\int_0^r \frac{\theta(s)}{\sqrt{(r^2-s^2)}}\,\mathrm{d}s. \tag{A.3}$$

A.2. General expression for the gap

We derive Eq. (15) from Eq. (14)

$$h(r) \equiv u(r) - \delta + f(r) \tag{A.4}$$

$$= \frac{2}{\pi}\left\{\int_0^a \mathrm{d}s\, \frac{\delta - \delta_0(s)}{\sqrt{r^2-s^2}} - \frac{\pi}{2}(\delta - f(r)) + \int_a^r \mathrm{d}s\, \frac{\theta(s)}{\sqrt{r^2-s^2}}\right\} \tag{A.5}$$

$$= \frac{2}{\pi}\left\{\int_a^r \mathrm{d}s\, \frac{\delta_0(s) - \delta}{\sqrt{r^2-s^2}} + \int_a^r \mathrm{d}s\, \frac{\theta(s)}{\sqrt{r^2-s^2}}\right\} \tag{A.6}$$

$$= \frac{2}{\pi}\left\{\int_a^r \mathrm{d}s\, \frac{\delta_0(s) - \delta_0(a)}{\sqrt{r^2-s^2}} + \int_a^r \mathrm{d}s\, \frac{\theta(s) - \theta(a)}{\sqrt{r^2-s^2}}\right\}, \tag{A.7}$$

where the equality of Eq. (A.5) and (A.6) results from the inversion of the definition of δ_0 (cf. Eq. (6) and its inverse Eq. (A.2)). In the case of the paraboloidal indenter, the first term is the Hertz gap Eq. (16).

Let us investigate the behaviour of the gap $h(r)$ for $r \to a(t)$. For $r = a(1+\varepsilon)$, one can show that, for a differentiable function $j(s)$,

$$\int_a^r \mathrm{d}s \, \frac{j(s)}{\sqrt{r^2 - s^2}} = (2\varepsilon)^{1/2} j(a) + O(\varepsilon^{3/2}). \tag{A.8}$$

Thus, continuity of θ at a entails that the second term in Eq. (15) behaves as $\varepsilon^{3/2}$ at a. The Hertz term $h_{\mathrm{Hertz}}(r,a)$ behaves similarly, since it as the same form (Eq. (16)), and therefore the $O(\varepsilon^{3/2})$ behaviour applies to the total gap.

Appendix B. Adhesive contact models

We derive the main results of the double-Hertz model in the elastic case before extending the results to the viscoelastic case.

B.1. Elastic case

B.1.1. Stress

In the double-Hertz model, the normalized stress distribution outside the contact zone is ellipsoidal:

$$\sigma(r) = \begin{cases} -\sigma_0 \sqrt{\dfrac{c^2 - r^2}{c^2 - a^2}} & \text{if } a \leqslant r \leqslant c, \\ 0 & \text{if } c < r. \end{cases} \tag{B.1}$$

We calculate g outside the contact zone: from Eq. (A.2) we infer that for $a \leqslant r \leqslant c$

$$g'(r) = -\frac{\pi}{2} \frac{\sigma_0}{\sqrt{c^2 - a^2}} r, \tag{B.2}$$

so that

$$g(r) = \begin{cases} \dfrac{\pi}{4} \sigma_0 \dfrac{r^2 - c^2}{\sqrt{c^2 - a^2}} & \text{if } a \leqslant r \leqslant c, \\ 0 & \text{if } c < r. \end{cases} \tag{B.3}$$

B.1.2. Penetration

From Eqs. (13) and (B.3), we obtain the displacement

$$\delta = \delta_0(a) - \frac{\pi \sigma_0}{4\mathscr{K}} \sqrt{c^2 - a^2}. \tag{B.4}$$

B.1.3. Force

For a paraboloidal indenter and a double-Hertz model, the inner term is

$$F_{\mathrm{int}} = \frac{8\mathscr{K} a^3}{3R} - \pi \sigma_0 a \sqrt{c^2 - a^2}. \tag{B.5}$$

In a double-Hertz model,

$$F_{\text{ext}} = \frac{\pi\sigma_0}{\sqrt{c^2 - a^2}} \left(-\frac{2}{3} c^3 - \frac{1}{3} a^3 + c^2 a \right). \tag{B.6}$$

Altogether,

$$F(a) = \frac{8\mathscr{K} a^3}{3R} - \frac{2\pi\sigma_0}{3} \frac{c^3 - a^3}{\sqrt{c^2 - a^2}}. \tag{B.7}$$

B.1.4. The gap

With Eqs. (15) and (9), and using the relation

$$Y(c - s)(s^2 - c^2) - (a^2 - c^2) = Y(s - c)(c^2 - s^2) + (s^2 - a^2), \tag{B.8}$$

where Y is the Heaviside step function, we have

$$h(r) = h_{\text{Hertz}}(r, a) + \frac{\sigma_0}{2\mathscr{K}\sqrt{c^2 - a^2}} \int_a^r \frac{(s^2 - a^2) - Y(s - c)(s^2 - c^2)}{\sqrt{r^2 - s^2}} \, \mathrm{d}s \tag{B.9}$$

$$= h_{\text{Hertz}}(r, a) + \frac{\sigma_0}{2\mathscr{K}\sqrt{c^2 - a^2}} \left[\int_a^r \frac{(s^2 - a^2)}{\sqrt{r^2 - s^2}} - Y(r - c) \int_c^r \frac{(s^2 - c^2)}{\sqrt{r^2 - s^2}} \, \mathrm{d}s \right] \tag{B.10}$$

$$= h_{\text{Hertz}}(r, a) + \frac{\sigma_0}{2\mathscr{K}\sqrt{c^2 - a^2}} \{ f_{\text{H}}(r, a) - Y(r - c) f_{\text{H}}(r, c) \}, \tag{B.11}$$

where f_{H} is defined by Eq. (17). Combining these expressions

$$h(r) = \left(\frac{2}{\pi R} + \frac{\sigma_0}{2\mathscr{K}\sqrt{c^2 - a^2}} \right) f_{\text{H}}(r, a) - \frac{\sigma_0}{2\mathscr{K}\sqrt{c^2 - a^2}} Y(r - c) f_{\text{H}}(r, c). \tag{B.12}$$

B.1.5. Self-consistent approach

The first term only in Eq. (B.12) contributes to the integral. We have to calculate

$$I = \int_a^c \mathrm{d}r \sqrt{c^2 - r^2} \, \frac{\partial}{\partial r} f_{\text{H}}(r, a). \tag{B.13}$$

It can be shown that

$$I = \frac{\pi}{6} I_{\text{H}}(c, a) \tag{B.14}$$

with

$$I_{\text{H}}(c, a) = (c - a)^2 (c + 2a). \tag{B.15}$$

Thus

$$w = \left(\frac{2}{\pi R} + \frac{\sigma_0}{2\mathscr{K}\sqrt{c^2 - a^2}} \right) \frac{\sigma_0}{\sqrt{c^2 - a^2}} I \tag{B.16}$$

and

$$w = \frac{1}{3}\left(\frac{1}{R} + \frac{\pi\sigma_0}{4\mathscr{K}\sqrt{c^2 - a^2}}\right)\frac{\sigma_0}{\sqrt{c^2 - a^2}}\, I_{\mathrm{H}}(c, a). \tag{B.17}$$

B.1.6. Normalization

In the case of the sphere, we define

$$K = \frac{8\mathscr{K}}{3}. \tag{B.18}$$

Following Maugis (1992), we normalize F by πwR, and introduce

$$P = \frac{F}{\pi wR}, \tag{B.19}$$

$$A = \frac{a}{(\pi wR^2/K)^{1/3}}, \tag{B.20}$$

$$\Delta = \frac{\delta}{(\pi^2 w^2 R/K^2)^{1/3}}, \tag{B.21}$$

$$\lambda = \frac{2\sigma_0}{(\pi wK^2/R)^{1/3}}. \tag{B.22}$$

Then

$$G(S) = \frac{\pi}{3}\lambda\frac{S^2 - C^2}{\sqrt{C^2 - A^2}}, \tag{B.23}$$

$$\Delta = A^2 - \frac{\pi}{3}\lambda\sqrt{C^2 - A^2}, \tag{B.24}$$

$$P = A^3 - \frac{\pi}{3}\lambda\frac{C^3 - A^3}{\sqrt{C^2 - A^2}} \tag{B.25}$$

and

$$H(R) = \frac{2}{\pi}\left\{\left(1 + \frac{\pi}{3}\lambda\frac{1}{\sqrt{C^2 - A^2}}\right) f_{\mathrm{H}}(R, A) - \frac{\pi}{3}\lambda\frac{1}{\sqrt{C^2 - A^2}}\, Y(R - C) f_{\mathrm{H}}(R, C)\right\}, \tag{B.26}$$

$$1 = \frac{\pi}{6}\lambda\left(1 + \frac{\pi}{3}\lambda\frac{1}{\sqrt{C^2 - A^2}}\right)\frac{I_{\mathrm{H}}(C, A)}{\sqrt{C^2 - A^2}}. \tag{B.27}$$

B.2. Viscoelastic bodies—increasing contact radius

B.2.1. Displacement

The surface stress outside the contact zone ($a(t) < r$) is now given by

$$\sigma(r, t) = \begin{cases} -\sigma_0\sqrt{\dfrac{c(t)^2 - r^2}{c(t)^2 - a(t)^2}} & \text{if } a(t) < r < c(t), \\ 0 & \text{if } c(t) < r. \end{cases} \tag{B.28}$$

From Eq. (31), the penetration is given by

$$\delta(t) = \delta_0(a(t)) - \frac{\pi}{4}\,\sigma_0 \int_{t_{c\_}(a(t))}^{t} \mathrm{d}\tau\, \phi(t-\tau)\,\frac{\partial}{\partial\tau}\,\frac{c^2(\tau)-a^2(t)}{\sqrt{c^2(\tau)-a^2(\tau)}} \tag{B.29}$$

or, in normalized form,

$$\Delta(t) = A^2(t) - \frac{\pi}{3}\,\lambda \int_{t_{c\_}(A(t))}^{t} \mathrm{d}\tau\, \phi(t-\tau)\,\frac{\partial}{\partial\tau}\,\frac{C^2(\tau)-A^2(t)}{\sqrt{C^2(\tau)-A^2(\tau)}}. \tag{B.30}$$

B.2.2. Gap

In this case, Eq. (33) becomes

$$h(r,t) = h_{\mathrm{Hertz}}(r,t) + \frac{\sigma_0}{2}\int_{t_{c\_}(a(t))}^{t} \mathrm{d}\tau\, \phi(t-\tau)\,\frac{\partial}{\partial\tau}\,\frac{[f_{\mathrm{H}}(r,a(t)) - Y(r-c(\tau))f_{\mathrm{H}}(r,c(\tau))]}{\sqrt{c^2(\tau)-a^2(\tau)}} \tag{B.31}$$

or, in normalized form,

$$H(R,t) = \frac{2}{\pi}\left\{ f_{\mathrm{H}}(R,A(t)) + \frac{\pi}{3}\,\lambda \int_{t_{c\_}(A(t))}^{t} \mathrm{d}\tau\, \phi(t-\tau)\,\frac{\partial}{\partial\tau} \times \frac{[f_{\mathrm{H}}(R,A(t)) - Y(R-C(\tau))f_{\mathrm{H}}(R,C(\tau))]}{\sqrt{C^2(\tau)-A^2(\tau)}} \right\}. \tag{B.32}$$

B.2.3. Self-consistency

We compute

$$w = \int_{a(t)}^{c(t)} \sigma(r,t)\,\frac{\mathrm{d}}{\mathrm{d}r}\,h(r,t)\,\mathrm{d}r. \tag{B.33}$$

This first term in Eq. (B.31) contributes as in the elastic case, or

$$\frac{\sigma_0}{3R\sqrt{c(t)^2-a(t)^2}}\,I_{\mathrm{H}}(c(t),a(t)). \tag{B.34}$$

The second term contributes

$$\frac{\sigma_0^2}{2\sqrt{c(t)^2-a(t)^2}} \int_{t_{c\_}(a(t))}^{t} \mathrm{d}\tau\, \phi(t-\tau)\,\frac{\partial}{\partial\tau}\left[\frac{1}{\sqrt{c(\tau)^2-a(\tau)^2}} \int_{a(t)}^{c(t)} \mathrm{d}r\sqrt{(c(t)^2-r^2)}\,\frac{\partial}{\partial r}\,[f_{\mathrm{H}}(r,a(t) - Y(r-c(\tau))f_{\mathrm{H}}(r,c(\tau))]\right] \tag{B.35}$$

and the self-consistency equation is

$$w = \frac{\sigma_0}{3\sqrt{c(t)^2 - a(t)^2}} \left\{ \frac{1}{R} I_{\mathrm{H}}(c(t), a(t)) \right.$$
$$\left. + \frac{\pi\sigma_0}{4} \int_{t_{c\_}(a(t))}^{t} \mathrm{d}\tau\, \phi(t-\tau)\, \frac{\partial}{\partial\tau} \frac{I_{\mathrm{H}}(c(t), a(t)) - I_{\mathrm{H}}(c(t), c(\tau))}{\sqrt{c(\tau)^2 - a(\tau)^2}} \right\} \tag{B.36}$$

or, in normalized form,

$$1 = \frac{\pi\lambda}{6\sqrt{C(t)^2 - A(t)^2}} \left\{ I_{\mathrm{H}}(C(t), A(t)) \right.$$
$$\left. + \frac{\pi\lambda}{3} \int_{A(t)}^{t} \mathrm{d}\tau\, \phi(t-\tau)\, \frac{\partial}{\partial\tau} \frac{I_{\mathrm{H}}(C(t), A(t)) - I_{\mathrm{H}}(C(t), C(\tau))}{\sqrt{C(\tau)^2 - A(\tau)^2}} \right\}. \tag{B.37}$$

B.3. Viscoelastic bodies—decreasing contact radius

B.3.1. Displacement

The normalized form of Eq. (41) is

$$0 = \int_{t_{a\_}(A(t))}^{t} \mathrm{d}\tau\, \tilde{\psi}(t-\tau)\, \frac{\mathrm{d}}{\mathrm{d}\tau} \{\Delta(\tau) - \Delta_0(A(t))\}$$
$$+ \frac{\pi}{3}\lambda \left[\sqrt{C^2(t) - A^2(t)} + \int_{0}^{t_{a\_}(A(t))} \mathrm{d}\tau\, \tilde{\psi}(t-\tau)\, \frac{\mathrm{d}}{\mathrm{d}\tau} \right.$$
$$\left. \times \int_{0}^{\tau} \mathrm{d}\tau'\, \tilde{\phi}(\tau - \tau')\, \frac{\mathrm{d}}{\mathrm{d}\tau'} \frac{A^2(t) - C^2(\tau')}{\sqrt{C^2(\tau') - A^2(\tau')}} \right]. \tag{B.38}$$

B.3.2. The gap and the self-consistency relation

Due to the intertwining of time and space dependances, we introduce an equivalent form for the gap

$$h(r) = h_{\mathrm{Hertz}}(r, a) + u_{\mathrm{JKR}}(r, a) + u_{\mathrm{ext}}(r, a), \tag{B.39}$$

where in Eq. (15), we single out the JKR term in the gap equation

$$u_{\mathrm{JKR}}(r, a) = -\frac{2}{\pi}\, \theta(a) \arccos\left(\frac{a}{r}\right) \tag{B.40}$$

and

$$u_{\mathrm{ext}}(r, a) = \frac{2}{\pi} \int_{a}^{r} \mathrm{d}s\, \frac{\theta(s)}{\sqrt{r^2 - s^2}}. \tag{B.41}$$

From Eq. (42), we are led to split $u_{\rm ext}$ into three terms

$$u_{\rm ext} = u_{\rm ext1} + u_{\rm int1}, + u_{\rm int2}, \tag{B.42}$$

with

$$u_{\rm ext1} = \int_0^t \mathrm{d}\tau\, \phi(t-\tau)\, \frac{\partial}{\partial \tau} \int_{\max(a(t),a(\tau))}^{r} \mathrm{d}s\, \frac{g(s,\tau)}{\sqrt{r^2-s^2}}, \tag{B.43}$$

$$u_{\rm int1} = \int_{t_{a\_}(a(t))}^{t} \mathrm{d}\tau\, \phi(t-\tau)\, \frac{\partial}{\partial \tau} \int_{t_{a\_}(a(t))}^{\tau} \mathrm{d}\tau'\, \psi(\tau-\tau')\, \frac{\partial}{\partial \tau'} \times \int_{a(t)}^{\min(r,a(\tau),a(\tau'))} \mathrm{d}s\, \frac{\theta(s,\tau')}{\sqrt{r^2-s^2}}, \tag{B.44}$$

$$u_{\rm int2} = \int_{t_{a\_}(a(t))}^{t} \mathrm{d}\tau\, \phi(t-\tau)\, \frac{\partial}{\partial \tau} \int_{0}^{t_{a\_}(\min(r,a(\tau)))} \mathrm{d}\tau'\, \psi(\tau-\tau')\, \frac{\partial}{\partial \tau'} \int_0^{\tau'} \mathrm{d}\tau''\, \phi(\tau'-\tau'')\, \frac{\partial}{\partial \tau''} \int_{\max(a(t),a(\tau''))}^{\min(r,a(\tau))} \mathrm{d}s\, \frac{g(s,\tau'')}{\sqrt{r^2-s^2}}. \tag{B.45}$$

Introducing

$$f_t(r,d,e,f) \equiv \int_e^{\min(f,r)} \frac{(d-s^2)}{\sqrt{r^2-s^2}}\, \mathrm{d}s = f_d(r,d,e) - Y(r-f) f_d(r,d,f) \tag{B.46}$$

with

$$f_d(r,d,e) \equiv \int_e^r \frac{(d-s^2)}{\sqrt{r^2-s^2}}\, \mathrm{d}s = \left\{ -\frac{e}{2}\sqrt{r^2-e^2} - \left(\frac{r^2}{2} - d\right) \arccos\left(\frac{e}{r}\right) \right\}, \tag{B.47}$$

then, in the case of the double-Hertz model, the three spatial integrals in Eqs. (B.43)–(B.45) are, respectively,

$$I_{\rm ext1} = -\frac{\pi}{4}\, \sigma_0\, \frac{f_t(r, c^2(\tau), \max(a(t), a(\tau)), c(\tau))}{\sqrt{c^2(\tau) - a^2(\tau)}}, \tag{B.48}$$

$$I_{\rm int1} = f_t(r, \delta(\tau'), a(t), \min(a(\tau), a(\tau'))), \tag{B.49}$$

$$I_{\rm int2} = -\frac{\pi}{4}\, \sigma_0\, \frac{f_t(r, c^2(\tau''), \max(a(t), a(\tau')), a(\tau))}{\sqrt{c^2(\tau'') - a^2(\tau'')}}. \tag{B.50}$$

B.3.3. Self-consistency

We calculate

$$w = \int_{a(t)}^{c(t)} \sqrt{c(t)^2 - r^2}\, \frac{\partial}{\partial r}\, h(r,t)\, \mathrm{d}r. \tag{B.51}$$

The core of the calculation is

$$I_d(a,c,d,e) = \int_a^c \mathrm{d}r\, \sqrt{c^2 - r^2}\, \frac{\partial}{\partial r}\, f_d(r,d,e)$$
$$= -\frac{1}{3}(c^2 - a^2)^{3/2} \arccos\left(\frac{e}{a}\right) + e\left(d - \frac{c^2}{3}\right) I_3(a,c,e)$$
$$- \frac{2e}{3} I_5(a,c,e), \tag{B.52}$$

where

$$I_3(a,c,e) = \frac{\pi}{2}\left(\frac{c}{e} - 1\right) - \left\{\frac{c}{e} \arctan\frac{t_-}{e} - \arctan t_-\right\}, \tag{B.53}$$

$$I_5(a,c,e) = \frac{c^2 - e^2}{2}\left\{\frac{\pi}{2} - \frac{t_-}{1 + t_-^2} - \arctan t_-\right\} \tag{B.54}$$

with

$$t_- = \sqrt{\frac{a^2 - e^2}{c^2 - a^2}}. \tag{B.55}$$

Finally, in normalized form, the self-consistency equation is

$$1 = \frac{\lambda}{\sqrt{C(t)^2 - A(t)^2}}\left(T_d + \frac{\pi}{3}\lambda T_\sigma\right) \tag{B.56}$$

with

$$T_d = I_{\mathrm{H}}(C(t), A(t)) - \frac{\pi}{2}(C(t) - A(t))(\Delta(t) - \Delta_0(A(t))) + A_{\mathrm{int1}} \tag{B.57}$$

and

$$T_\sigma = A_{\mathrm{ext1}} + A_{\mathrm{int2}}. \tag{B.58}$$

$$A_{\mathrm{ext1}} = -\left[\int_{t_{c-}(A(t))}^{t_{a-}(C(t))} \mathrm{d}\tau + \int_{t_{a+}(C(t))}^{t} \mathrm{d}\tau\right]$$
$$\times\left[\phi(t-\tau)\frac{\mathrm{d}}{\mathrm{d}\tau}\frac{1}{\sqrt{C^2(\tau) - A^2(\tau)}}\{I_d(A(t), C(t), C^2(\tau), \max(A(t), A(\tau)))\right.$$
$$\left. - Y(C(t) - C(\tau)) I_d(A(t), C(t), C^2(\tau), C(\tau))\}\right], \tag{B.59}$$

$$A_{\mathrm{int1}} = \int_{t_{a-}(A(t))}^{t} \mathrm{d}\tau\, \phi(t-\tau)\frac{\mathrm{d}}{\mathrm{d}\tau}\int_{t_{a-}(A(t))}^{\tau} \mathrm{d}\tau'\, \psi(\tau - \tau')\frac{\mathrm{d}}{\mathrm{d}\tau'}$$
$$\times\{I_d(A(t), C(t), \Delta(\tau'), A(t)))$$
$$- Y(c(t) - \min(A(\tau), A(\tau')) I_d(A(t), C(t), \Delta(\tau'), \min(A(\tau), A(\tau')))\} \tag{B.60}$$

and

$$A_{\text{int2}} = -\int_{t_{a\_}(A(t))}^{t} \mathrm{d}\tau\, \phi(t-\tau)\, \frac{\mathrm{d}}{\mathrm{d}\tau} \int_0^{t_{a\_}(\min(C(t),A(\tau)))} \mathrm{d}\tau'\, \psi(\tau-\tau')\, \frac{\mathrm{d}}{\mathrm{d}\tau'}$$
$$\times \int_0^{\tau'} \mathrm{d}\tau''\, \phi(\tau'-\tau'')\, \frac{\partial}{\partial\tau''}\, \frac{1}{\sqrt{C^2(\tau'')-A^2(\tau'')}}$$
$$\times \{I_d(A(t), C(t), C^2(\tau''), \max(A(t), A(\tau')))$$
$$-Y(C(t)-A(\tau))I_d(A(t), C(t), C^2(\tau''), A(\tau))\}. \tag{B.61}$$

B.4. Viscoelastic bodies—the force

As in Section B.1.3, the total force is the sum of the outer term

$$F_{\text{ext}}(t) = \frac{\pi\sigma_0}{\sqrt{c^2(t)-a^2(t)}} \left\{ -\frac{2}{3}\, c^3(t) - \frac{1}{3}\, a^3(t) + a(t)c^2(t) \right\} \tag{B.62}$$

and the inner term

$$F_{\text{int}}(t) = F_{\text{int},a}(t) + F_{\text{int},b}(t) \tag{B.63}$$

with

$$F_{\text{int},a}(t) = 4 \int_0^t \mathrm{d}\tau\, \psi(t-\tau)\, \frac{\mathrm{d}}{\mathrm{d}\tau} \int_0^{\min(a(t),a(\tau))} \mathrm{d}r\, (\delta(\tau) - \delta_0(r)) \tag{B.64}$$

and

$$F_{\text{int},b}(t)$$
$$= 4 \int_0^{t_{a\_}(a(t))} \mathrm{d}\tau\, \psi(t-\tau)\, \frac{\mathrm{d}}{\mathrm{d}\tau} \int_0^{\tau} \mathrm{d}\tau'\, \phi(\tau-\tau')\, \frac{\mathrm{d}}{\mathrm{d}\tau'} \int_{a(\tau)}^{a(t)} \mathrm{d}r\, g(r,\tau') \tag{B.65}$$
$$= \pi\sigma_0 \int_0^{t_{a\_}(a(t))} \mathrm{d}\tau\, \psi(t-\tau)\, \frac{\mathrm{d}}{\mathrm{d}\tau} \int_0^{\tau} \mathrm{d}\tau'\, \phi(\tau-\tau')\, \frac{\mathrm{d}}{\mathrm{d}\tau'}$$
$$\times \frac{m-a(\tau)}{\sqrt{c^2(\tau')-a^2(\tau')}} \left\{ \frac{m^2+ma(\tau)+a(\tau)^2}{3} - c^2(\tau') \right\}, \tag{B.66}$$

where m stands for $\min(a(t), c(\tau'))$. In normalized form, we have

$$P = \frac{3}{2} \left\{ \int_0^t \mathrm{d}\tau\, \tilde{\psi}(t-\tau)\, \frac{\mathrm{d}}{\mathrm{d}\tau} \left(M_a \Delta(\tau) - \frac{M_a^3}{3} \right) \right.$$
$$\left. + \frac{\pi}{3}\, \lambda \left[\frac{1}{\sqrt{C^2(t)-A^2(t)}} \left\{ -\frac{2}{3}\, C^3(t) - \frac{1}{3}\, A^3(t) + A(t)C^2(t) \right\} \right.\right.$$

$$+\int_0^{t_{a-}(a(t))} \mathrm{d}\tau\, \tilde{\psi}(t-\tau)\,\frac{\mathrm{d}}{\mathrm{d}\tau}\int_0^{\tau}\mathrm{d}\tau'\,\tilde{\phi}(\tau-\tau')\,\frac{\mathrm{d}}{\mathrm{d}\tau'}$$

$$\times\frac{M-A(\tau)}{\sqrt{C^2(\tau')-A^2(\tau')}}\left\{\frac{M^2+MA(\tau)+A(\tau)^2}{3}-C^2(\tau')\right\}\Bigg]\Bigg\}, \tag{B.67}$$

where M_a stands for $\min(A(t),A(\tau))$ and M for $\min(A(t),C(\tau'))$.

References

Attard, P., 2001a. Interaction and deformation of viscoelastic particles. 2. Adhesive particles. Langmuir 17 (14), 4322–4328.

Attard, P., 2001b. Interaction and deformation of viscoelastic particles: nonadhesive particles. Phys. Rev. E 63 (6), 1604–1609.

Barthel, E., 1998a. On the description of the adhesive contact of spheres with arbitrary interaction potentials. J. Colloid Interface Sci. 200, 7.

Barthel, E., 1998b. Surface deformations, spring stiffness and the measurement of solvation forces. Thin Solid Films 330, 27.

Barthel, E., 1999. The adhesive contact of spheres: when the interaction is complex. Colloids Surf. A 149, 99.

Barthel, E., Lin, X.Y., Loubet, J.L., 1996. Adhesion energy measurements in the presence of adsorbed liquid using a rigid surface force apparatus. J. Colloid Interface Sci. 177, 401.

Boussinesq, J., 1885. Application des Potentiels à l'Etude de l'Equilibre et du Mouvement des Solides Elastiques. Paris.

Bradley, R.S., 1932. The cohesive energy between solid surfaces and the surface energy of solids. Philos. Mag. 13, 853.

Derjaguin, B.V., 1934. Untersuchungen ueber die reibung und adhaesion. Kolloid Z. 69, 155.

Derjaguin, B.V., Muller, V.M., Toporov, Y.P., 1975. On the role of molecular forces in contact deformation. J. Colloid Interface Sci. 53, 314.

Greenwood, J.A., 1997. Adhesion of elastic spheres. Proc. R. Soc. London A 453, 1277.

Greenwood, J.A., Johnson, K.L., 1981. The mechanics of adhesion of viscoelastic solids. Philos. Mag. 43, 697.

Greenwood, J.A., Johnson, K.L., 1998. An alternative to the Maugis model of adhesion between viscoelastic spheres. J. Phys. D: Appl. Phys. 31, 3279.

Hertz, H., 1882. Ueber die beruehrung fester elastische koerper. J. Reine. Angew. Math. 92, 156.

Hughes, B.D., 1980. Some applications of continuum mechanics in colloid and interface science. Ph.D. Thesis, ANU, Canberra.

Huguet, A.-S., Barthel, E., 2000. Surface forces and the adhesive contact of axisymmetric bodies. J. Adhesion 74, 143–175.

Hui, C.Y., Baney, J.M., Kramer, E.J., 1998. Contact mechanics and adhesion of viscoelastic spheres. Langmuir 14 (22), 6570–6578.

Johnson, K.L., 1999. Contact mechanics and the adhesion of viscoelastic spheres. In: Tsukruk, V.V., Wahl, K.J. (Eds.), Microstructure and Microtribology of Polymer Surfaces. ACS, Washington, DC.

Johnson, K.L., Kendall, K., Roberts, A.D., 1971. Surface energy and the contact of elastic solids. Proc. R. Soc. London A 324, 301.

Lantz, M.A., O'Shea, S.J., Welland, M.E., Johnson, K.L., 1997. Atomic-force microscope study of contact area and friction on NbSe2. Phys. Rev. B 55, 10776.

Lin, Y.Y., Hui, C.Y., Baney, J.M., 1999. Viscoelastic contract (sic), work of adhesion and the JKR technique. J. Phys. D: Appl. Phys. 32 (17), 2250–2260.

Lin, Y.Y., Hui, C.Y., Jagota, A., 2001. The role of viscoelastic adhesive contact in the sintering of polymeric particles. J. Colloid Interface Sci. 237 (2), 267–282.
Lowengrub, M., Sneddon, I.N., 1965. The effect of internal pressure on a penny-shaped crack at the interface of two bonded dissimilar elastic half-spaces. Int. J. Eng. Sci. 3, 451.
Maugis, D., 1992. Adhesion of spheres: the JKR–DMT transition using a dugdale model. J. Colloid Interface Sci. 150, 243.
Maugis, D., Gauthier-Manuel, B., 1994. JKR–DMT transition in the presence of a liquid meniscus. J. Adhesion Sci. Technol. 8, 1311.
Muller, V.M., Yushenko, V.S., Derjaguin, B.V., 1980. On the influence of molecular forces on the deformation of an elastic sphere and its sticking to a rigid plane. J. Colloids Interface Sci. 77, 91.
Muller, V.M., Yushchenko, V.S., Derjaguin, B.V., 1982. General theoretical considerations on the influence of surface forces on contact deformations. J. Colloid Interface Sci. 92, 92.
Schapery, R.A., 1975a. A theory of crack initiation and growth in viscoelastic media: analysis of continuous growth. Int. J. Fracture 11, 549–562.
Schapery, R.A., 1975b. A theory of crack initiation and growth in viscoelastic media: approximate method of analysis. Int. J. Fracture 11, 369–388.
Schapery, R.A., 1975c. A theory of crack initiation and growth in viscoelastic media: theoretical development. Int. J. Fracture 11, 141–159.
Schapery, R.A., 1989. On the mechanics of crack closing and bonding in linear viscoelastic media. Int. J. Fracture 39, 163.
Sneddon, I.N., 1951. Fourier Transform. New York.
Sneddon, I.N., 1965. The relation between load and penetration in the axisymmetric boussinesq problem for a punch of arbitrary profile. Int. J. Eng. Sci. 3, 47.
Tabor, D., 1977. Surface forces and surface interactions. J. Colloids Interface Sci. 58, 2.
Ting, T.C.T., 1966. The contact stresses between a rigid indenter and a viscoelastic half-space. J. Appl. Mech. 33, 845.